Original Research

White Matter Changes in Primary Dystonia Determined by 2D Distribution Analysis of Diffusion Tensor Images

An Vo, PhD,[1] David Eidelberg, MD,[1] and Aziz M. Uluğ, PhD[1,2]*

Purpose: To determine brain tissue affected by dystonia by making group comparison of parameter-based diffusion tensor imaging (DTI) distributions of patients with control subjects. A 2D distribution analysis of mean diffusivity and fractional anisotropy index was used for modeling brain tissues according to the inherent diffusion characteristics.

Materials and Methods: Seven affected carriers of the DYT1 dystonia mutation and eight healthy control subjects were imaged for a previous study. We employed a 2D distribution analysis of all the diffusion voxels and a four compartmental brain model for group comparison of the dystonia subjects and controls.

Results: Our analysis showed disease involvement in the white matter of the patients. Excellent tissue characterization was achieved automatically using the 2D distribution analysis based on a physical brain model.

Conclusion: This 2D analysis implicated white matter in dystonia and could be useful as a screening tool in diseases with unknown pathologies.

Key Words: MRI; DTI; DYT1; 2D distribution; dystonia
J. Magn. Reson. Imaging 2013;37:59–66.

DIFFUSION TENSOR IMAGING (DTI) has been used extensively to investigate the properties of brain tissues at different levels of architectural organization and to diagnose many diseases (1,2). The most commonly used DTI parameters are mean diffusivity (MD or D_{av}) and fractional anisotropy index (FA).

Previously, studies investigated the use of DTI to characterize normal and pathological tissues (3–7) according to the diffusion characteristics. In these studies, whole-brain mean diffusivity histograms were obtained from the entire brain. The whole-brain histogram data can be modeled by three (3,5,7) compartments each described by a one-dimensional (1D) Gaussian function. The first compartment represents the brain tissue consisting of white and gray matter. The second compartment is brain tissue mixed with cerebrospinal fluid (CSF) (ie, partial volume compartment) and the third compartment consists of CSF. One disadvantage of this 1D modeling utilizing only the average diffusion constant is that white and gray matter cannot be distinguished from each other since average diffusion constants of these are similar. In order to differentiate white and gray matter, a whole-brain FA histogram can be used instead. But there is still a considerable overlap of FA values in these tissue types, and usually prior to the distribution analysis, segmentation of the brain is necessary using an additional image set T1-weighted registered to the DTI images. The prior removing of CSF voxels may also be necessary by using the additional image set.

Despite its limitations, 1D whole-brain diffusion histograms have been used extensively in the past, including in studies of breast imaging (8), aging (3,9,10), multiple sclerosis (4), brain maturation (5,11), traumatic brain injury (12–14), intracranial hemorrhage (15), lupus (7,16), chemoirradiation damage (17), Parkinson's disease (18), and Batten's disease (19). A distribution analysis tool that can differentiate the tissues according to the inherent diffusion characteristics (5,20–22) can be useful, especially in the diseases that cause microstructural damage, or have a nonfocal disease burden.

2D histogram analysis of DTI has been used previously to segment white and gray matter (WM and GM) (23). In that work, each tissue class (WM, GM, and CSF) was assumed to be modeled by a 2D Gaussian surface. In another work that used DTI for tissue segmentation (24), mean diffusivity was used to classify CSF and non-CSF tissue, and FA was used to classify WM and non-WM tissues.

In this study we used 2D distribution analysis of DTIs with a four-compartmental physical brain model (WM, GM, CSF, and mixture). Each tissue class was also modeled by a 2D Gaussian function. FA and diffusion constant information from each voxel were determined and used concurrently in four 2D

[1]Center for Neurosciences, The Feinstein Institute for Medical Research, Manhasset, New York, USA.
[2]Department of Radiology, Albert Einstein College of Medicine, Bronx, New York, USA.
*Address reprint requests to: A.M.U., Center for Neurosciences, The Feinstein Institute for Medical Research, 350 Community Dr., Manhasset, NY 11030. E-mail: ulug@ieee.org
Received January 23, 2012; Accepted August 6, 2012.
DOI 10.1002/jmri.23805
View this article online at wileyonlinelibrary.com.

Gaussians describing the tissue types. The analysis included a fourth compartment (mixture) to account for partial-volume voxels as well as pathology.

We applied this 2D distribution analysis on previously acquired DTI data from carriers of DYT1 mutation for primary dystonia (25). Clinical magnetic resonance imaging (MRI) of dystonia subjects normally do not show any pathology. Primary dystonia is a brain disorder in which affected individuals exhibit abnormal involuntary twisting movements and abnormal postures of the trunk and limbs (26). Hereditary dystonia has been associated with over 10 distinct genetic mutations. The DYT1 mutation is the most common of these and is inherited as an autosomal dominant trait, with a clinical penetrance rate of ~30%. Although the pathology of hereditary dystonias is not completely understood, the disorder is thought to involve abnormalities of neural pathways linking the cerebellum to the basal ganglia-thalamo-cortical motor regions (25,27,28). To demonstrate the applicability of this method to the investigation of brain diseases, the fitted parameters of the four-compartment brain model were used for comparison of DYT1 gene carriers and control subjects. We also segmented brain tissue according to the diffusion characteristics to look for obvious pathology.

MATERIALS AND METHODS

2D Gaussian Functions

We used a 2D Gaussian function of both D_{av} and FA to model a brain compartment of a single tissue type. A 2D distribution of the entire brain is then fitted using four 2D Gaussian functions describing the WM, GM, CSF, and partial volume/mixture compartment as:

$$f(D_{av},FA)=K\sum_{i=1}^{4}C_i(2\pi)^{-1}\det(\overline{\overline{V}}_i)^{-\frac{1}{2}} \times\exp\left\{-\frac{1}{2}[D_{av}-D_i \quad FA-FA_i]\overline{\overline{V}}_i^{-1}\begin{bmatrix}D_{av}-D_i\\FA-FA_i\end{bmatrix}\right\}, \quad [1]$$

where for each compartment i,

$$\overline{\overline{V}}_i=\begin{bmatrix}V_{11} & V_{12}\\ V_{21} & V_{22}\end{bmatrix}_i \quad [2]$$

is the 2 × 2 covariance matrix of each Gaussian function.

$$\begin{gathered}V_{11}=E(D_{av}^2)-(E(D_{av}))^2,\\ V_{12}=V_{21}=E(D_{av}FA)-E(D_{av})E(FA), \quad \text{and}\\ V_{22}=E(FA^2)-(E(FA))^2\end{gathered} \quad [3]$$

where $E(X)=\sum_n x_nP(x_n)$ is the expected value of variable X (the estimate of population mean based on the model); x_n is the outcome with probability $P(x_n)$. K is the total number of brain voxels in the distribution. Four 2D Gaussian functions (i =1,2,3,4) represent WM, GM, CSF, and mixture compartments, respectively. Using the above Eq. [1], 2D distribution can be modeled by parameters of $\{C_i, D_i, FA_i, \overline{\overline{V}}_i\}$, where $i=1,2,3,4$, and $\sum_{i=1}^{4}C_i=1$.

For each compartment i, C_i represents the proportion of volume in that compartment; D_i and FA_i are the mean values of D_{av} and FA.

Parameter Estimation Using EM Algorithm

Each pair value of D_{av} and FA at a given voxel is considered to be a 2D vector observation $\overline{x}(k)$. Hence, the dataset $X=\{\overline{x}(1),\ldots,\overline{x}(N)\}$ contains N 2D vector observations, where N is the number of voxels of the 3D D_{av} and FA maps. We assume that each data point $\overline{x}(k)$ is independent and identically distributed (i.i.d: each data point is a random variable which has the same probability distribution as the others and all are mutually independent):

$$f(\overline{x}\setminus P)=K\sum_{i=1}^{4}C_if_i(\overline{x}\setminus p_i), \quad [4]$$

where $P=\{C_1, C_2, C_3, C_4, p_1, p_2, p_3, p_4\}$. Each component is a 2D Gaussian function with its own parameters $p_i=\{\overline{\mu}_i, \overline{\overline{V}}_i\}$ as follows:

$$f_i(\overline{x}\setminus p_i)=(2\pi)^{-1}\det(\overline{\overline{V}}_i)^{-\frac{1}{2}}\exp\left[-\frac{1}{2}(\overline{x}-\overline{\mu}_i)^T\overline{\overline{V}}_i^{-1}(\overline{x}-\overline{\mu}_i)\right], \quad [5]$$

where $\overline{x}=\begin{bmatrix}D_{av}\\FA\end{bmatrix}$, $\overline{\mu}=\begin{bmatrix}D_i\\FA_i\end{bmatrix}$, and T is the transpose operation. Expectation maximization algorithm (EM) (29–31, http://www1.aston.ac.uk/eas/research/groups/ncrg/resources/netlab/), is an iterative optimization method to estimate unknown parameters P, given observation data X. Unknown parameters P are obtained by maximizing their posterior probability given the data X as follows:

$$P^*=\arg\max_P f(P\setminus X). \quad [6]$$

Data Acquisition

DTIs were collected from seven affected carriers of the DYT1 dystonia mutation (four males, three females, age 46.8 ± 15.4) and eight healthy control subjects (five males, three females, age 39.7 ± 19.3). Images were acquired with a 3T GE whole-body MR scanner with an 8-channel head coil in parallel imaging mode with an acceleration factor of 2 (25). A single-shot spin-echo EPI sequence was used, with one image without diffusion weighting and 55 isotropically distributed diffusion gradient directions. The b-value in the diffusion-weighted images was 1000 s/mm^2 (=1 msec/μm^2). The DTI protocol included 72 slices of 1.8 mm thickness, field of view (FOV) of 230 mm, image matrix was 128 × 128 zero-filled to 256 × 256. TE was 68.3 msec and TR was 7000 msec. The nominal image resolution was (0.9 × 0.9 × 1.8) mm^3.

Data Analysis

After DTI data acquisition, diffusion images were processed using FSL routines (http://

www.fmrib.ox.ac.uk/fsl/). First, eddy current correction using affine registration to the b_0 ($b = 0$) image was applied to all DTIs for correction of eddy current distortions and simple head motion. Next, we used the brain extraction tool (BET) of FSL to remove non-brain tissue such as the skull in b_0 image and to create a brain mask. Using the eddy current corrected DTI scans and the brain mask, we calculated D_{av} (=Trace/3) and FA maps for all brain voxels.

2D Distribution Analysis

Using a physical diffusion brain model of four compartments (WM, GM, CSF, and mixture compartment), 2D distribution was fitted using four 2D Gaussian functions as described above. Parameters of 2D distribution were fitted using the EM algorithm (http://www1.aston.ac.uk/eas/research/groups/ncrg/ resources/netlab/). Diffusion D_{av} was measured between 0 and 5 μm^2/ms and FA was defined between 0 and 1.

Group Comparison

Diffusion tensor data for each subject was modeled by 25 parameters (24 free parameters since $\sum C_i = 1$): {K, C_i, D_i, FA_i, V_{11},V_{12}, V_{22}, and $i = 1,2,3,4$. We computed the mean and standard deviation of parameters in each group. Two-tailed t-test was used to determine the significance of the group differences. The threshold for significance was set at $P < 0.05$. To account for false positives due to multiple comparisons of the three parameters in each compartment, we utilized Bonferroni correction in determining significance.

We used the covariance matrix $\overline{\overline{V}}_i$ as a first step to implicate the compartments in the dystonia group that are significantly different from the controls. Then we used the fitted diffusion parameters {C_i, D_i, FA_i} to further discriminate the compartment involved in the disease process.

Brain Segmentation Using 2D Distribution of DTI Data

We segmented the four compartments using fitted 2D distribution of DTI data as shown in Fig. 5 for a control subject. With all obtained parameters $\{C_i, D_i, FA_i, \overline{\overline{V}}_i\}$, we performed classification for all data points $X = \{\overline{x}(1), \ldots, \overline{x}(N)\}$. A data point $\overline{x}(k) = [D_{av}(k), FA(k)]^T$ of a voxel is determined to belong to a compartment i when the contribution from the i^{th} compartment has the maximum contribution to the voxel, ie, $i = \arg\max_{j=1,\ldots,4} C_j f_j(\overline{x}(k))$.

In order to compare the brain segmentation results using 2D distribution analysis with the common segmentation method, we used a standard segmentation tool (FAST) in FSL to segment b_0 image with T2-weighted contrast into three tissue types (GM, WM, and CSF). This segmentation method is based on a hidden Markov random field model and an associated EM algorithm (32). In the b_0 image, skull and non-brain tissue were first removed by using the brain extraction tool in FSL (33) before the segmentation.

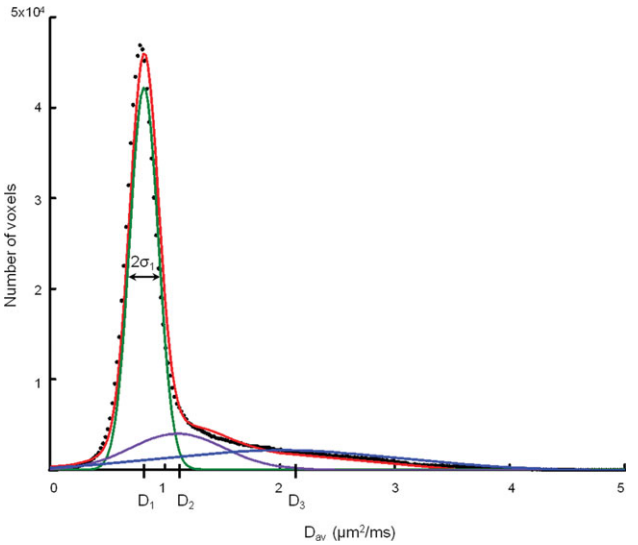

Figure 1. Histogram of diffusion tensor data D_{av} and fitted 1D distribution using three 1D Gaussian functions. The histogram bin size is 0.02 μm^2/ms. The black dots are data points from the histogram bins. The red line is the overall fit to the data. D_1 is the mean and σ_1 is the standard deviation of the first compartment. The means of the second compartment (D_2) and the third compartment (D_3) are also shown. [Color figure can be viewed in the online issue, which is available at wileyonlinelibrary.com.]

1D and 2D Distribution Comparison

To compare the 2D distribution results with 1D distribution analysis, we processed D_{av} of the healthy control subjects and the DYT1 carriers with 1D distribution analysis (3,5). Histograms of D_{av} are fitted to three 1D Gaussian functions (5) as follows:

$$f(D_{av}) = \sum_{i=1}^{3} W_i \exp\left[-\left(\frac{D_{av} - D_i}{\sigma_i}\right)^2\right]. \quad [7]$$

Each subject was modeled by nine parameters {W_i, D_i, σ_i} where i=1,2,3, including mean D_i, standard deviation σ_i and weighting coefficients W_i corresponding to three Gaussian functions of all compartments. Figure 1 shows the 1D distribution of D_{av} fitted with three 1D Gaussian functions (3,5).

RESULTS

Figure 2 shows the 2D distribution for each group. Here, the 2D distribution data for the entire group of subjects is visualized using a 2D histogram of 100 × 100 bins. The bin size is 0.05 μm^2/ms × 0.01. Figure 3 shows the average fitted contours of the individual compartments for each group of subjects. We calculated the parameters of the covariance matrix for each compartment and summarized them in Table 1. The fitted diffusion parameters of C_i, D_i, FA_i, when i=1,2,3,4, and the total number of brain voxels, K, obtained from the two groups are summarized in Table 2. Figure 4 shows standard segmentation (32) of b_0 image from a control subject. The four compartments of the brain are also visualized by segmentation in Fig. 5 using the 2D distribution of DTI data in the

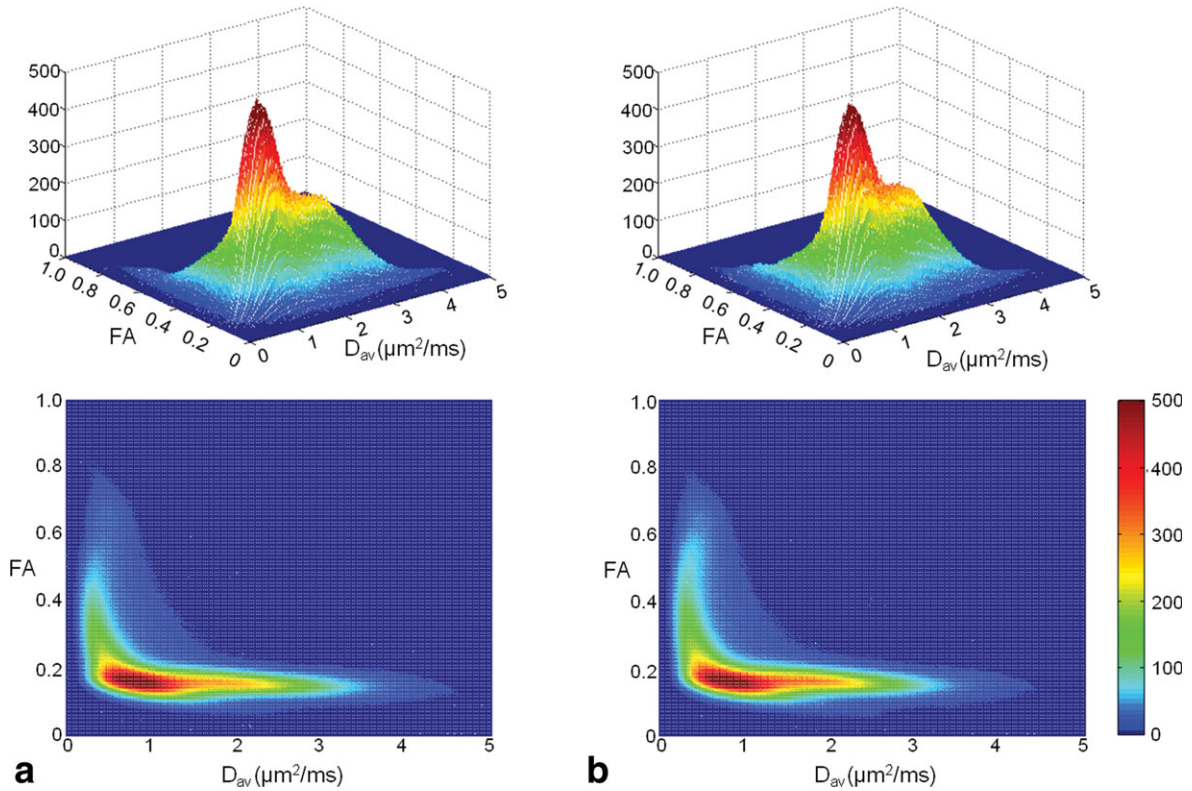

Figure 2. 2D distributions (FA, D_{av}) of subject groups are shown. Here the 2D distribution data for the entire group of subjects is visualized using a 2D histogram of 100 × 100 bins. The bin size is 0.05 μm^2/ms × 0.01. **a**: Control group. **b**: Dystonia group.

same control subject of Fig. 4. The segmented images in Fig. 5 that depend on the diffusion characteristics of the brain model visualized the basal ganglia structures better than the standard segmentation of b_0 images which are shown in Fig. 4. Diffusion parameters of the 1D distribution are summarized in Table 3.

Table 1 lists significant changes of the parameters of the covariance matrix. The changes in the WM (V_{22}, $P < 0.009$ corrected) and the mixture compartments (V_{11}, $P < 0.03$ corrected) point to disease involvement in these two compartments. Since V_{22} is the variance of FA, the significant change in V_{22} in the WM compartment points to a pathological process whereby WM coherence is altered. V_{11} is the variance of D_{av}, and V_{11} changes in the mixture compartment may suggest a change in the composition of this compartment. In addition, in the CSF compartment one parameter of the covariance matrix was changed, but

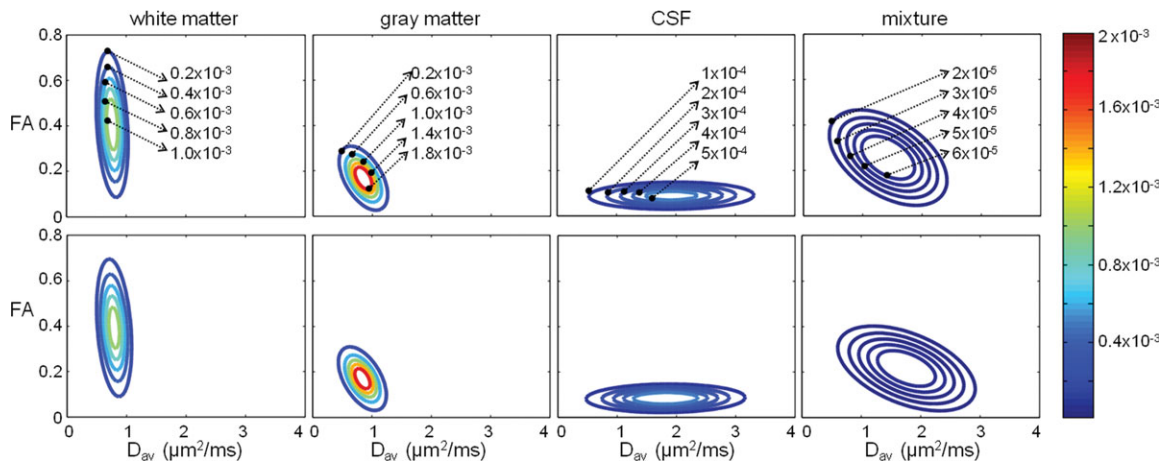

Figure 3. The average fitted 2D Gaussian contours of the individual compartments for each group. The distribution of each subject is decomposed into the individual compartments and then the average fitted parameters for each group are computed. Top row shows the control group and bottom row is the dystonia DYT1 gene carrier group. Left to right: compartment 1 to compartment 4. Contour levels are included in the figure.

Table 1
Fitted Parameters of the Covariance Matrix of Each 2D Gaussian Function

	Model parameters	Control group ($n = 8$) mean ± SD	DYT1 group ($n = 7$) mean ± SD	*P*
First compartment	V_{11}	0.019 ± 0.0062	0.024 ± 0.0116	ns
(White matter)	V_{12}	−0.006 ± 0.0022	−0.007 ± 0.0050	ns
	V_{22}	0.028 ± 0.0011	0.026 ± 0.0014	0.003*
Second compartment	V_{11}	0.033 ± 0.0063	0.033 ± 0.0039	ns
(Gray matter)	V_{12}	−0.006 ± 0.0012	−0.006 ± 0.0006	ns
	V_{22}	0.004 ± 0.0003	0.004 ± 0.0002	ns
Third compartment	V_{11}	0.539 ± 0.0580	0.465 ± 0.0776	0.03
(CSF)	V_{12}	0.001 ± 0.0010	0.001 ± 0.0016	ns
	V_{22}	0.001 ± 0.0003	0.001 ± 0.0002	ns
Mixture compartment	V_{11}	0.356 ± 0.0849	0.500 ± 0.1299	0.01*
(White + gray + CSF)	V_{12}	−0.036 ± 0.0186	−0.039 ± 0.0151	ns
	V_{22}	0.016 ± 0.0069	0.013 ± 0.0083	ns

*Significant after the Bonferroni correction in each compartment.

this change was not significant when corrected for multiple comparisons.

Table 2 points to a significant increase in D_1 and decrease in FA_1 in the WM compartment of the dystonia group when compared with the controls. There were no significant group differences in the GM and CSF compartments, suggesting that DYT1 dystonia is associated with WM changes. When corrected for multiple comparisons in each compartment, FA_1 is still significantly different in the patient group ($P < 0.03$, corrected) when compared to the control group. There were also significant changes in the mixture compartment similar to those observed in the WM compartment (D_i and FA_i). These changes were not significant when Bonferroni corrected.

The 1D analysis only showed a significant change in σ_2 in the mixture compartment ($P < 0.03$), and a marginal increase ($P = 0.09$, two-tailed *t*-test) in the first compartment diffusion value (Table 3). When corrected for multiple comparisons, the change in σ_2 was not significant ($P < 0.09$, corrected).

DISCUSSION

There are significant differences between the dystonia and normal groups in terms of the measured parameters (Tables 1, 2). When corrected for multiple comparisons the covariance matrix parameters (Table 1) point to pathological changes in the WM compartment and mixture compartment. Further changes in Table 2 point to the WM as the only significantly different compartment when corrected for multiple comparisons (FA_1, $P < 0.01$, corrected). In the first compartment (WM) the D_1 of dystonia group is marginally increased, and the FA_1 decreased when compared with the control group. This result suggests WM involvement in DYT1 dystonia, where subtle damage to the fiber tracts became evident in the group analysis. Similarly, the mixture compartment shows D_4 increase and FA_4 decrease. Although these (D_4 and FA_4) changes are not significant when corrected for multiple comparisons, these results may suggest some evidence for pathological tissue in the patient group since the brain model will classify any tissue

Table 2
Fitted Parameters of the 2D Distribution of Diffusion Tensor Data

	Model parameters	Control group ($n = 8$) mean ± SD	DYT1 group ($n = 7$) mean ± SD	*P*
	K	1048190 ± 71369	1107479 ± 175438	ns
First compartment	C_1	0.395 ± 0.016	0.397 ± 0.032	ns
(White matter)	D_1	0.766 ± 0.022	0.791 ± 0.031	0.05
	FA_1	0.406 ± 0.011	0.393 ± 0.009	0.01*
Second compartment	C_2	0.338 ± 0.038	0.321 ± 0.029	ns
(Gray matter)	D_2	0.848 ± 0.015	0.839 ± 0.027	ns
	FA_2	0.167 ± 0.007	0.170 ± 0.007	ns
Third compartment	C_3	0.195 ± 0.048	0.209 ± 0.049	ns
(CSF)	D_3	1.922 ± 0.082	1.817 ± 0.306	ns
	FA_3	0.089 ± 0.010	0.084 ± 0.005	ns
Mixture compartment	C_4	0.072 ± 0.018	0.073 ± 0.011	ns
(White + gray + CSF)	D_4	1.428 ± 0.171	1.760 ± 0.368	0.02
	FA_4	0.256 ± 0.037	0.216 ± 0.047	0.04

Diffusion constants (D_i) were measured in (μm^2/ms) and FA is defined between 0 and 1. K is the number of voxels used in the analysis in each subject. C_i is the proportion of voxels in the given compartment. D_i is the mean of average diffusion constant and FA_i is the mean of FA in a given compartment.
*Significant after the Bonferroni correction.

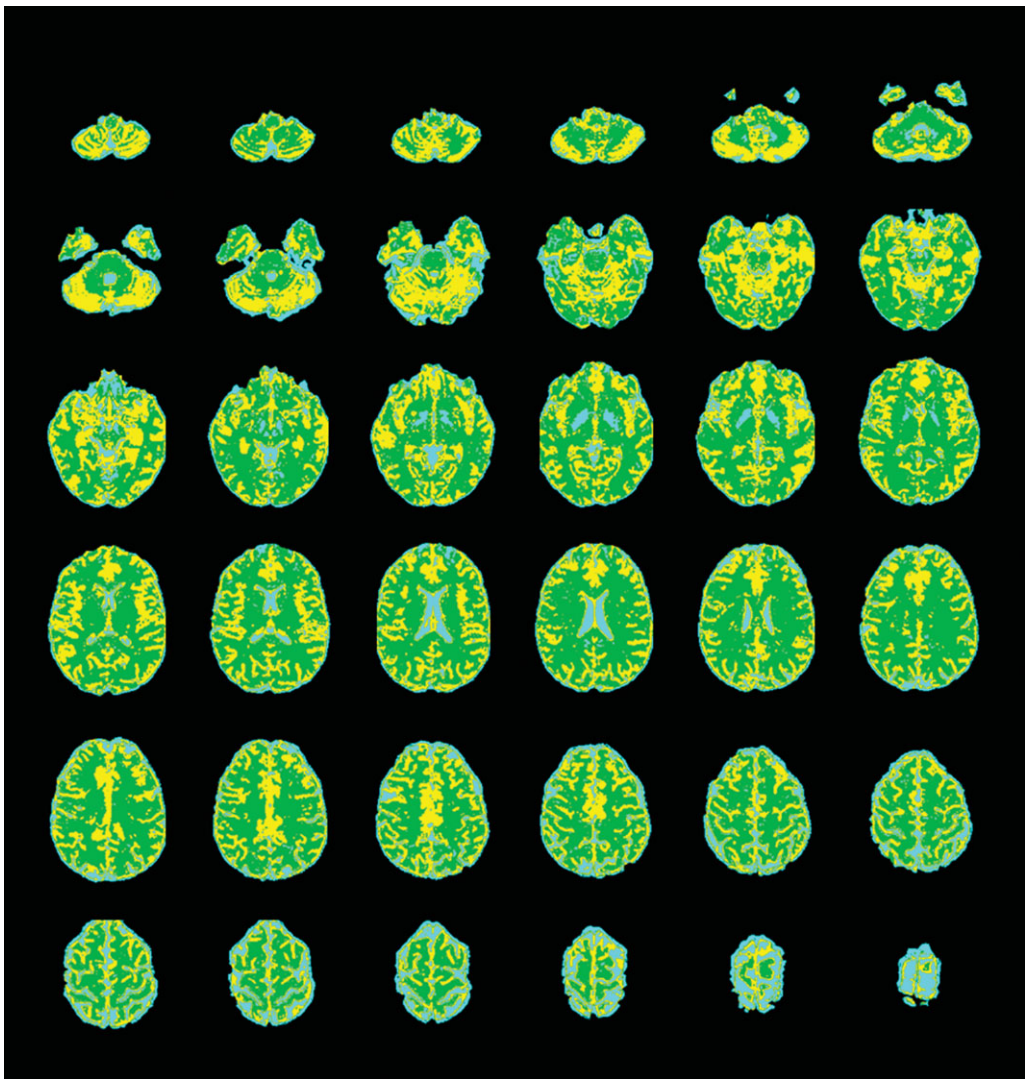

Figure 4. b_0 (T2-weighted contrast) image of a control subject (same subject as in Fig. 5) was segmented using FAST segmentation algorithm in FSL (32). The first compartment (white matter) is shown in green, the second (gray matter) in yellow, the third (CSF) in blue. [Color figure can be viewed in the online issue, which is available at wileyonlinelibrary.com.]

that cannot be identified as WM, GM, or CSF as part of the mixture compartment.

Table 3 shows the 1D distribution analysis results. The D_1 increase in the first compartment, which includes both WM and GM of the patient group, does not reach significance. The 2D method where WM and GM tissues can be separately investigated is more sensitive to pathological changes than the 1D distribution analysis. The change in the second compartment, which is the mixture compartment of the 1D distribution analysis, is in agreement with the 2D analysis mixture compartment and may be evidence for the existence of pathological tissue that has different inherent diffusion properties than WM and GM. Similar to the 2D distribution analysis, in the 1D distribution analysis voxels which cannot be classified as brain tissue (WM and GM) and CSF will be included in the mixture compartment. This finding is not significant when Bonferroni correction is applied.

Figure 5 provides visual confirmation of the physical diffusion brain model of the four compartments. The 2D distribution analysis-based segmented images display excellent tissue classification. Figure 4 shows segmented images using the standard segmentation method (32) based on b_0 (T2-weighted contrast) images used for the same subject as in Fig. 5. The segmented images that depend on the diffusion characteristics of the brain model are better than the segmentation of b_0 images especially in the basal ganglia structures. In addition to the three tissue types, the brain model-based segmented images visualized a fourth compartment of mixture mainly around the ventricles. Although in Fig. 5 the fourth compartment visualized only the voxels with considerable partial-volume content as designed, the fourth compartment can also be useful in visualizing pathological voxels where the diffusion characteristics were significantly different than WM and GM.

In the 1D distribution of D_{av}, each subject was modeled by nine parameters. When these nine parameters of the model of dystonia group were compared with the control group (Table 3) there was, however,

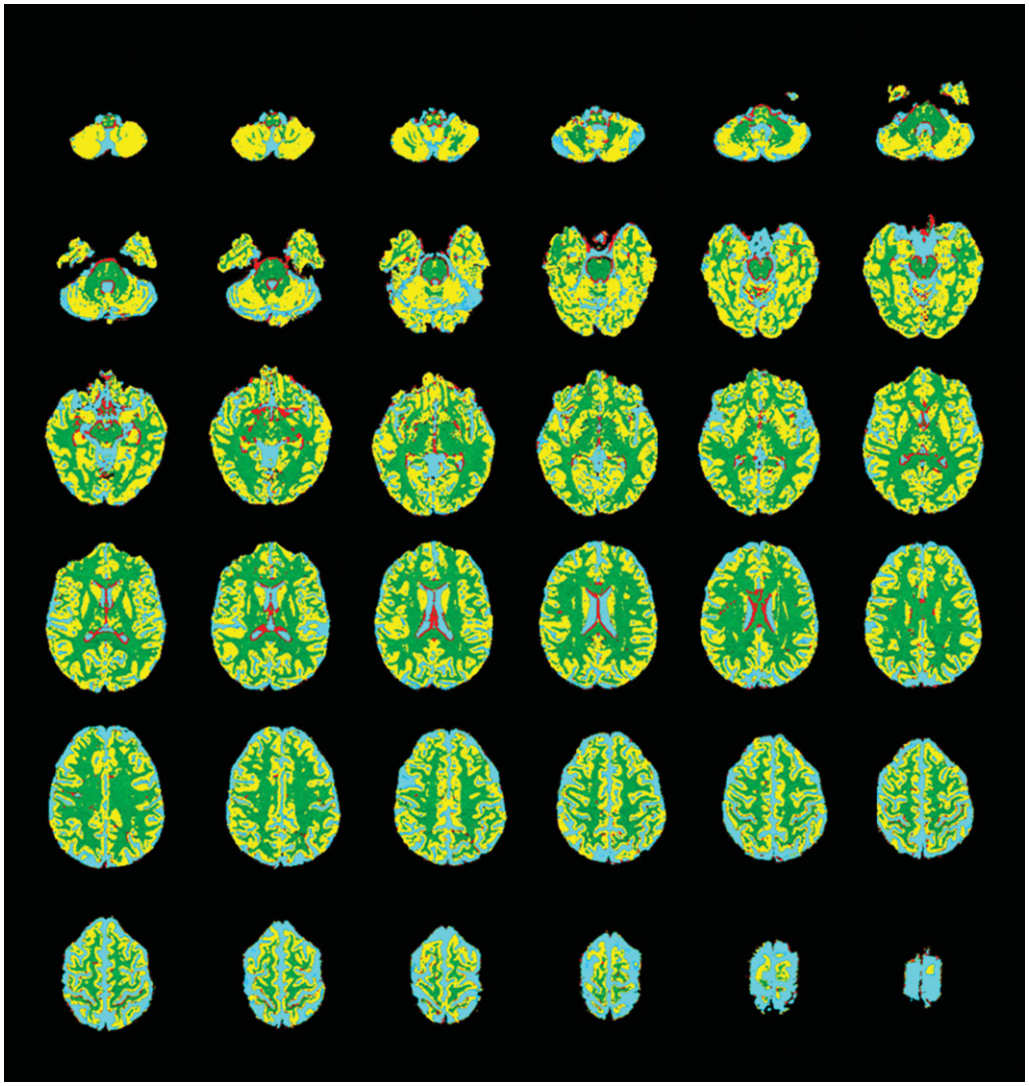

Figure 5. Segmentation results of a control subject using the 2D distribution of diffusion tensor imaging data and the brain model are shown. The first compartment (white matter) is shown in green, the second (gray matter) in yellow, the third (CSF) in blue, and the last (mixture) in red. [Color figure can be viewed in the online issue, which is available at wileyonlinelibrary.com.]

only one significant feature (σ_2) with $P < 0.05$. With the 2D distribution, we obtained seven significantly different features with $P < 0.05$. When Bonferroni correction was applied in each compartment, there were no significantly different features in the 1D analysis, and one significant feature in the 2D analysis pointing to WM involvement in the dystonia group. The covariance matrix also has two significant features after Bonferroni correction pointing to WM involvement and changes in the mixture compartment. It is clear that

Table 3
Fitted Parameters of the 1D Distribution of Diffusion Tensor Data, D_{av}

	Model parameters	Control group ($n = 8$) mean ± SD	DYT1 group ($n = 7$) mean ± SD	P
First compartment	W_1	42470 ± 6436	42832 ± 7463	ns
(Brain tissue: white and gray matter)	D_1	0.782 ± 0.020	0.801 ± 0.029	ns ($P = 0.09$)
	σ_1	0.182 ± 0.015	0.186 ± 0.024	ns
Second compartment	W_2	4649 ± 1497	4218 ± 977	ns
(Brain tissue and CSF)	D_2	1.181 ± 0.091	1.213 ± 0.138	ns
	σ_2	0.380 ± 0.084	0.537 ± 0.195	0.03
Third compartment	W_3	2086 ± 496	2077 ± 663	ns
(CSF)	D_3	1.838 ± 0.246	2.056 ± 0.503	ns
	σ_3	1.118 ± 0.219	1.092 ± 0.322	ns

Diffusion constants (D_i) were measured in μm^2/ms. 1D histograms were computed with 250 bins. The bin size is 0.02 μm^2/ms.

the 2D distribution analysis reveals more information about the brain than the 1D histograms.

The results show that brain tissue can be characterized by inherent diffusion parameters using distribution analysis in 2D. This method provides excellent segmentation based on the diffusion parameters. We found considerable differences between the two groups studied in terms of the parameters measured, pointing to a clear WM involvement in dystonia. Considering that dystonia is not known to affect the brain globally, this finding is significant and is compatible with the presence of highly localized tract-specific changes on DTI scans (25,28,34).

In conclusion, we described a 2D distribution analysis of the DTI data. We investigated the utility of the proposed methodology in a group of dystonia patients carrying the disease-related DYT1 mutation. The analysis showed WM involvement in this disease. Excellent tissue characterization was achieved automatically using the 2D distribution analysis based on a physical brain model. This completely automated analysis can help in aiding the diagnosis of dystonia and in elucidating the pathophysiology of this disorder. We expect this 2D analysis to be useful as a screening tool in diseases with unknown pathologies, such as neuropsychiatric disorders, that can point to brain tissue with possible disease involvement.

ACKNOWLEDGMENT

We thank Dr. Maren Carbon-Correll for valuable discussions and acquisition of diffusion tensor images.

REFERENCES

1. Le Bihan D, Mangin JF, Poupon C, et al. Diffusion tensor imaging: concepts and applications. J Magn Reson Imaging, Special Issue: European Special Issue 2001;13:534–546.
2. Basser PJ, Jones DK. Diffusion-tensor MRI: theory, experimental design and data analysis—a technical review. NMR in Biomed Special Issue 2002;15:456–467.
3. Chun T, Filippi CG, Zimmerman RD, et al. Diffusion changes in the aging human brain. AJNR Am J Neuroradiol 2000;21: 1078–1083.
4. Cercignani M, Inglese M, Pagani E, et al. Mean diffusivity and fractional anisotropy histograms of patients with multiple sclerosis. AJNR Am J Neuroradiol 2001;22:952–958.
5. Ulug AM. Distribution analysis of diffusion tensor data. In: Proc 10th Annual Meeting ISMRM, Honolulu; 2002:1141.
6. Heim S, Hahn K, Sämann PG, et al. Assessing DTI data quality using bootstrap analysis. Magn Reson Med 2004;52:582–89.
7. Zhang L, Harrison M, Heier LA, et al. Diffusion changes in patients with systemic lupus erythematosus. Magn Reson Imaging 2007;25:399–405.
8. Englander SA, Uluğ AM, Brem R, et al. Diffusion imaging of human breast. NMR Biomed 1997;10:348–352.
9. Nusbaum AO, Tang CY, Buchsbaum MS, et al. Regional and global changes in cerebral diffusion with normal aging. AJNR Am J Neuroradiol 2001;22:136–142.
10. Rovaris M, Iannucci G, Cercignani M, et al. Age-related changes in conventional, magnetization transfer, and diffusion-tensor MR imaging findings: study with whole-brain tissue histogram analysis. Radiology 2003;227:731–738.
11. Zhang L, Thomas KM, Davidson MC, et al. MR quantitation of volume and diffusion changes in the developing brain. AJNR Am J Neuroradiol 2005;26:45–49.
12. Zhang L, Ravdin LD, Relkin N, et al. Increased diffusion in the brain of professional boxers: a preclinical sign of traumatic brain injury. AJNR Am J Neuroradiol 2003;24:52–57.
13. Inglese M, Makani S, Johnson G, et al. Diffuse axonal injury in mild traumatic brain injury: a diffusion tensor imaging study. J Neurosurg 2005;103:298–303.
14. Benson RR, Meda SA, Vasudevan S, et al. Global white matter analysis of diffusion tensor images is predictive of injury severity in traumatic brain injury. J Neurotrauma 2007;24:446–459.
15. Kamal AK, Dyke JP, Katz JM, et al. Temporal evolution of diffusion after spontaneous supratentorial intracranial hemorrhage. AJNR Am J Neuroradiol 2003;24:895–901.
16. Bosma GP, Huizinga TW, Mooijaart SP, et al. Abnormal brain diffusivity in patients with neuropsychiatric systemic lupus erythematosus. AJNR Am J Neuroradiol 2003;24:850–854.
17. Leung LH, Ooi GC, Kwong DL, et al. White matter diffusion anisotropy after chemo-irradiation: a statistical parametric mapping study and histogram analysis. NeuroImage 2004;21: 261–268.
18. Tessa C, Giannelli M, Della Nave R, et al. A whole-brain analysis in de novo Parkinson disease. AJNR Am J Neuroradiol 2008;29: 674–680.
19. Dyke JP, Voss HU, Sondhi D, et al. Assessing disease severity in late infantile neuronal cerois lipofuscinosis using quantitative MR diffusion-weighted imaging. AJNR Am J Neuroradiol 2007;28: 1232–1236.
20. Ulug AM. Monitoring brain development with quantitative diffusion tensor imaging. Dev Sci 2002;5:286–292.
21. Ulug AM, Vo A, Argyelan M, et al. 2-D distribution analysis of diffusion tensor imaging data of dystonia patients. In: Proc ESMRI Biology Congress (ESMRMB) 2009:154.
22. Vo A, Argyelan M, Eidelberg D, et al. 2-D distribution analysis of DTI in two phenotypes of dystonia patients. In: Proc 18th Annual Meeting ISMRM, Stockholm; 2010.
23. Cercignani M, Inglese M, Siger-Zajdel M, et al. Segmenting brain white matter, gray matter and cerebro-spinal fluid using diffusion tensor-MRI derived indices. Magn Reson Imaging 2001;19: 1167–1172.
24. Liu T, Li H, Wong K, et al. Brain tissue segmentation based on DTI data. Neuroimage 2007;38:114–123.
25. Argyelan M, Carbon M, Niethammer M, et al. Cerebellothalamocortical connectivity regulates penetrance in dystonia. J Neurosci 2009;29:9740–9747.
26. Tanabe LM, Kim CE, Alagem N, et al. Primary dystonia: molecules and mechanisms. Nat Rev Neurol 2009;5:598–609.
27. Niethammer M, Carbon M, Argyelan M, et al. Hereditary dystonia as a neurodevelopmental circuit disorder: evidence from neuroimaging. Neurobiol Dis 2011;42:202–209.
28. Ulug AM, Vo A, Argyelan M, et al. Cerebello-thalamo-cortical pathway abnormalities in torsinA DYT1 knock-in mice. Proc Natl Acad Sci U S A 2011;108:6638–6643.
29. Dempster A, Laird N, Rubin D. Maximum likelihood from incomplete data via the EM algorithm. J R Stat Soc Series B 1977;39: 1–38.
30. Hartley H. Maximum likelihood estimation from incomplete data. Biometrics 1958;14:174–194.
31. McLachlan G, Krishnan T. The EM algorithm and extensions. Wiley series in probability and statistics 1997. Hoboken, NJ: John Wiley & Sons.
32. Zhang Y, Brady M, Smith S. Segmentation of brain MR images through a hidden Markov random field model and the expectation maximization algorithm. IEEE Trans Med Imaging 2001;20: 45–57.
33. Smith S. Fast robust automated brain extraction. Hum Brain Mapp 2002;17:143–155.
34. Carbon M, Kingsley PB, Tang C, et al. Microstructural white matter changes in primarytorsion dystonia. Mov Disord 2008;23: 234–239.